Batteries & Supercaps

Research Article
doi.org/10.1002/batt.202500265

Chemistry Europe
European Chemical Societies Publishing

www.batteries-supercaps.org

Benchmarking Mg Electrolytes with Different Metal Plating/Stripping Protocols

Tjaša Pavčnik, Janja Šuster, Elena Tchernychova, Jan Bitenc,* and Robert Dominko

Over the past two decades, various Mg compounds have been explored in the search for electrolytes with the best electrochemical performance. While notable progress in electrolyte chemistry has been made, the field lacks evaluation protocols for studying electrolytes under closer-to-practical conditions. This work evaluates three generations of Mg electrolytes: organometallic, non-nucleophilic $Mg(TFSI)_2$-$MgCl_2$, and state-of-the-art Mg alkoxyborate/-aluminate electrolytes. Experiments performed under standard galvanostatic cycling show inferior performance of TFSI-based electrolytes compared to all-phenyl complex and $Mg[X(hfip)_4]_2$ (X = Al, B) electrolytes. To accelerate side reactions and Mg passivation, additional cycling protocols are introduced, namely, macroreversibility cycling and cycling with OCV rest periods after Mg plating. The latter demonstrates a decline in Coulombic efficiency in all tested electrolytes during OCV rest periods, pointing toward interphase stability as a critical point. The electrochemical analysis is complemented by SEM, EDX, and XPS characterization of Mg metal deposits. XPS results indicate that a more metallic Mg interphase does not necessarily correlate with improved Mg plating/stripping efficiency, emphasizing the key role of interphase composition. This work highlights the need to move beyond conventional laboratory cycling protocols to assess electrolyte stability under realistic conditions and provides a framework for more comprehensive future electrolyte evaluation.

1. Introduction

Over the last three decades, lithium-ion batteries (LIBs) have emerged as the dominant battery technology, powering a wide range of devices from smartphones and laptops to renewable energy systems and electric vehicles. Their ascendance is largely attributed to the enhanced gravimetric and volumetric energy densities over the previous battery technologies (such as lead–acid and nickel–cadmium batteries),[1] which facilitated the development of smaller, more compact battery configurations. However, LIBs typically depend on scarce material resources with uneven global distribution and still have limited recycling options, reducing their long-term viability. For a sustainable energy storage future, new complementary technologies are required. Multivalent batteries are considered a promising post-LIBs alternative.

Due to the low redox potential (–2.37 vs. standard hydrogen electrode, SHE) and high gravimetric and volumetric capacities of Mg metal (2206 mAh g^{-1} and 3834 mAh cm^{-3}, respectively), Mg batteries are one of the most investigated multivalent candidates.[2] Additionally, the Mg metal anode is less reactive than alkali metals and less prone to dendrite formation than Li metal, potentially improving battery safety.[3] With Mg ranking as the seventh most common element in the Earth's crust, Mg batteries could be generally more sustainable and cost-effective than currently dominant LIBs.[4] On the other hand, the development of Mg batteries is accompanied by many challenges. One of the critical ones is the passivation of the Mg metal anode with different electrolyte components (solvents, salts, impurities), resulting in the formation of an ion-blocking passivation layer, preventing reversible battery operation.[5] The requirement for high reductive stability on the Mg metal anode and high purity severely limits the number of Mg electrolyte candidates.

Since the early twenties of the previous century, when reversible Mg plating/stripping was demonstrated, a number of different electrolytes have been investigated. According to the historical development as well as some specific properties, Mg electrolytes can be divided into three generations (**Figure 1**). The first generation of practical Mg electrolytes was based on organometallic chloride-containing active species. The electrolytes typically consist of Grignard reagents (alkyl/aryl Mg halides) and their combination with Lewis acids, mixed in different ratios.[6,7] Due to the presence of reactive organometallic species, such electrolytes can act as scavengers for various contaminants that are present in the electrolyte (oxygen, water) or formed during cell operation (protonated species), preventing the formation of a blocking passive layer on the surface of the Mg metal anode.[8] Among different combinations, the best electrochemical performance was demonstrated by the so-called all-phenyl complex (APC) electrolyte, a mixture of

T. Pavčnik, E. Tchernychova, J. Bitenc, R. Dominko
Department of Materials Chemistry
National Institute of Chemistry
Hajdrihova 19, 1000 Ljubljana, Slovenia
E-mail: jan.bitenc@ki.si

T. Pavčnik, J. Šuster, J. Bitenc, R. Dominko
Faculty of Chemistry and Chemical Technology
University of Ljubljana
Večna pot 113, 1000 Ljubljana, Slovenia

R. Dominko
Alistore-European Research Institute
CNRS FR 3104
Hub de l'Energie, Rue Baudelocque, 80039 Amiens, France

Supporting information for this article is available on the WWW under https://doi.org/10.1002/batt.202500265

Research Article
doi.org/10.1002/batt.202500265
Chemistry Europe
European Chemical Societies Publishing

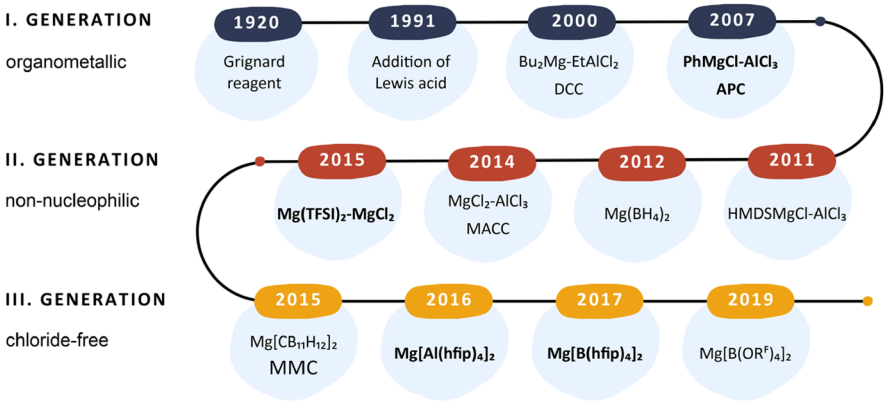

Figure 1. Timeline of the development of electrolytes for Mg batteries divided into three generations.

PhMgCl and $AlCl_3$ in a 2:1 ratio. The APC electrolyte enables Mg plating/stripping with low overpotentials and Coulombic efficiency above 99%, in addition to its high oxidative stability (> 3.3 V) and ionic conductivity (4–5 mS cm^{-1}).[9] The disadvantage of the first generation of electrolytes is their pyrophoric and nucleophilic character, which makes them incompatible with electrophilic cathode materials, such as sulfur.

Thus, the development is directed to less reactive electrolytes based on non-nucleophilic active species, representing the second generation of Mg electrolytes. Different non-nucleophilic-based electrolytes, such as HMDSMgCl (bis(hexamethyldisilazide)) and $Mg(TFSI)_2$ (bis(trifluoromethanesulfonyl)imide), showed limited cycling performance due to the poor reductive stability of anions and their decomposition on the Mg metal anode, resulting in gradual electrode passivation.[10,11] Improved electrochemical properties were observed upon the addition of inorganic chlorides ($MgCl_2$ or $AlCl_3$),[12,13] which mitigate the formation of the blocking passive layer and improve the reversibility of Mg plating/stripping.[14] Nevertheless, the Coulombic efficiency and overpotentials of non-nucleophilic electrolytes are inferior to Mg organohaloaluminate electrolytes of the first generation. The drawback of both (first and second) generations of Mg electrolytes is the presence of chloride ions, which are corrosive to common current collectors and cell casings and, as such, unsuitable for practical applications.[15]

The most recent generation of Mg electrolytes focuses on non-nucleophilic chloride-free electrolytes. Typical representatives contain boron-based anions, which were found to be highly compatible with the Mg anode.[16,17] Magnesium monocarborane or MMC electrolyte ($Mg[CB_{11}H_{12}]_2$) demonstrates good electrochemical performance in higher glymes (tri- and tetraglyme) but suffers from insufficient solubility in low molecular weight solvents like mono- and diglyme.[18] High viscosity and strong coordination observed in higher glymes pose challenges for high-power density applications due to the slow kinetics associated with hindered ion movement.[19] Currently, the most prominent candidates for ether-based Mg electrolytes are fluorinated alkoxyborates and alkoxyaluminates, with a general formula of $Mg[X(OR^F)_4]_2$ (X = B or Al, OR^F = fluorinated alkoxy group). Model electrolytes, $Mg[B(hfip)_4]_2$ and $Mg[Al(hfip)_4]_2$, demonstrate high ionic conductivity (in the range up to 10 mS cm^{-1}), and reversible Mg plating/stripping with Coulombic efficiency close to 99% and overpotentials below 0.1 V.[20,21] Since they are chloride-free and non-nucleophilic in character, electrolytes are compatible with non-noble current collectors and different cathode materials, which makes them the most viable candidates among the three generations of Mg electrolytes for practical Mg batteries.[17]

The electrochemical performance of electrolytes is typically evaluated through galvanostatic cycling, as it allows rather precise estimation of the practical Coulombic efficiency, the most common parameter to describe the degree of reversibility of plating/stripping processes. In a standard galvanostatic cycling, all of the plated Mg metal is stripped from the working electrode with each cycle. In the practical battery cell, this would relate to the metal anode-free battery cell configurations where the initial Mg ion source is limited and efficient cycling depends on the reversibility of Mg plating/stripping. In addition, the so-called "reservoir" or macroreversibility cycling has been developed that mimics the situation in practical cells with an excess metal anode while providing information about metal plating/stripping efficiency.[22] By stripping only a part of the initially plated metal, an excess of metal is present on the working electrode throughout the entire cycling experiment, amplifying the side reactions on the metal surface. The method was first introduced by Aurbach et al. for the investigation of lithium,[22] but has also been later used for the evaluation of Mg[23–25] and Zn metal plating/stripping.[26,27] To further probe the Mg metal anode under realistic conditions, our group proposed Mg plating/stripping experiments where open circuit voltage (OCV) rest periods are introduced after each Mg plating half-cycle.[17] This approach amplifies spontaneous metal passivation/corrosion processes due to an extended period of time during which the Mg metal deposit surface is exposed to the electrolyte. By exposing deposited Mg metal to the electrolyte under idle conditions, the OCV rest step simulates a practical scenario of load-free cell rest, enabling insight into chemical stability. All three above-mentioned cycling protocols were already used in a benchmark investigation of the effect of functional additives on the electrochemical performance of the $Mg[Al(hfip)_4]_2$ electrolyte.[17] The use of advanced cycling protocols, which put more focus on side reactions, is crucial to evaluate the applicability of electrolytes under practically relevant conditions.

Although APC, $Mg(TFSI)_2$, and $Mg[X(hfip)_4]_2$ (X = B and Al) electrolytes have been investigated before, the field lacks direct benchmarking of different generations of Mg electrolytes under

Research Article
doi.org/10.1002/batt.202500265
Chemistry Europe
European Chemical Societies Publishing

comparable conditions such as the concentration of the electrolyte, solvent type and quality, cell setup, and different cycling protocols. Within this work, we aim to fill this gap. Herein, we investigate the electrochemical performance of three generations of Mg electrolytes (**Figure 2**a), using three different cycling protocols (**Figure** 2b). Besides standard laboratory battery-testing protocol, macroreversibility and cycling with rest periods at OCV potential are employed, representing aggravated conditions and allowing the evaluation of electrolytes closer to practical conditions. The electrochemical characterization is complemented by the Mg deposit's surface investigation using scanning electron microscopy with energy dispersive X-ray spectroscopy (SEM-EDX) and X-ray photoelectron spectroscopy (XPS) characterization.

2. Results and Discussion

For a relevant electrochemical evaluation and benchmarking of different Mg electrolytes, it is essential to ensure comparable testing conditions. In terms of that, all electrolytes were prepared with the same concentration of Mg^{2+} species, specifically 0.4 M, which is relatively close to the optimum ion conductivity of the used salts, as well as a similar quality of solvents,[28] which were obtained through a multistep in-house purification procedure. A standard solvent for the APC electrolyte is tetrahydrofuran (THF),[9] whereas diglyme (G2) was used for the preparation of other electrolytes within this work. Diglyme was chosen for its good transport properties and favorable electrochemical performance compared to other glyme-based solvents.[11,20] While various current densities are used in the literature for Mg plating/stripping, typically in the range of 0.1–1 mA cm^{-2}, a current density of 1 mA cm^{-2} was selected in this work as it is closest to the current densities applied in practical batteries.

The electrochemical performance of the prepared electrolytes was first investigated under the standard galvanostatic cycling protocol, as shown in **Figure 3**. The APC electrolyte demonstrates Mg plating/stripping with the highest average Coulombic efficiency, exceeding 99%, consistent with the literature report.[9] $Mg[Al(hfip)_4]_2$ and $Mg[B(hfip)_4]_2$ electrolytes follow with somewhat lower efficiencies of 98.1% and 96.3%, respectively. The improved performance of the aluminate-based analog is attributed to better salt dissociation and enhanced transport properties compared to the borate-based electrolyte.[20] As the electrolyte containing only the $Mg(TFSI)_2$ salt shows very limited reversibility with high overpotentials,[11] electrolytes combining $Mg(TFSI)_2$ and $MgCl_2$ salts were employed. Notably, the stoichiometry of added chlorides is important. A higher proportion of inorganic chlorides, which are, in general, poorly soluble in higher glymes, can hinder complete salt dissolution,[11] whereas insufficient chloride fails to significantly improve the electrochemical properties of the electrolytes.[29] Within this work, we tested electrolytes with two different compositions, $Mg(TFSI)_2$:$MgCl_2$ in 1:1 and 1:0.5 ratios. Both $Mg(TFSI)_2$-based electrolytes show inferior performance compared to APC and $Mg[X(hfip)_4]_2$, with average Coulombic efficiencies of 90.6% (1:1) and 79.8% (1:0.5). Notably, the electrolyte with less chloride exhibits more than 10% lower Coulombic efficiency compared to the electrolyte with an equivalent ratio of TFSI- and Cl-based salts. This highlights the role of chloride ions in preventing side reactions during Mg plating/stripping. All electrolytes demonstrate lower Coulombic efficiency in the first 5–10 cycles, corresponding to the electrode activation and electrolyte conditioning, after which stable cycling is observed. In the $Mg[B(hfip)_4]_2$ electrolyte, minor deviations in Coulombic efficiency are also noted after initial cycling. This can be attributed to the selection of the working electrode, as our experiments were performed on stainless steel, while Pt foil as a working electrode is typically employed in laboratory tests. Indeed, the parallel measurement using $Mg[B(hfip)_4]_2$ electrolyte and Pt working electrode shows similar efficiency of Mg plating/stripping to stainless steel but significantly more stable Coulombic efficiency (Figure S1, Supporting Information), consistent with the literature reports.[21,30] The unstable Coulombic efficiency on stainless steel is likely observed due to the poor adhesion of the Mg deposits on the specific substrate, resulting

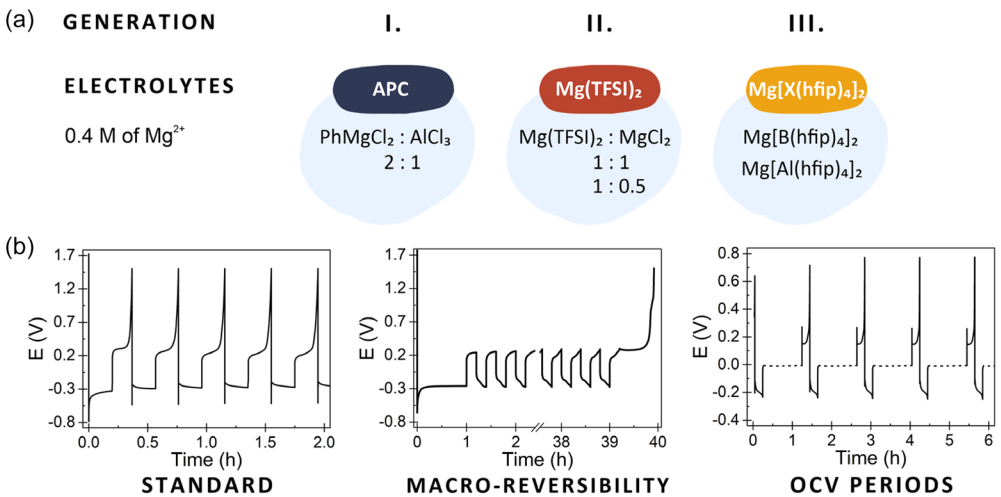

Figure 2. a) Selected electrolytes of three generations. b) Different cycling protocols (from left to right): standard galvanostatic cycling, macroreversibility cycling, and standard galvanostatic cycling with OCV periods (dashed lines) after each Mg plating half cycle.

Research Article
doi.org/10.1002/batt.202500265
Chemistry Europe
European Chemical Societies Publishing

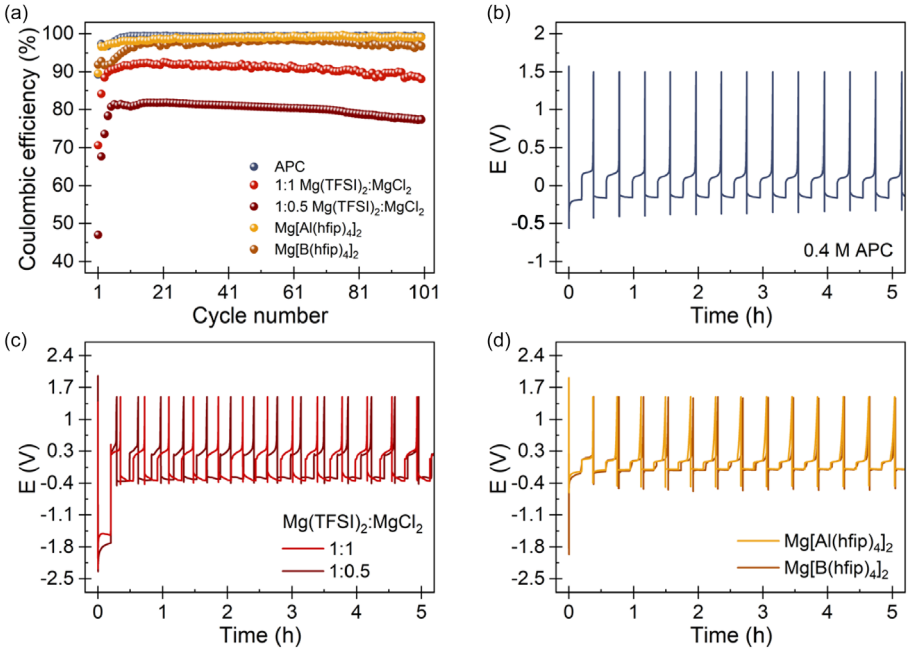

Figure 3. Comparison of standard galvanostatic cycling protocols. a) Coulombic efficiencies of Mg plating/stripping in selected electrolytes at 0.4 M concentration on stainless steel working electrode. b–d) Corresponding potential versus time profiles in the initial cycles for APC (b), $Mg(TFSI)_2$:$MgCl_2$ (c, 1:1 red, 1:0.5 brown), and $Mg[X(hfip)_4]_2$ electrolytes (d, X = Al yellow, X = B orange).

in an intermittent loss of contact with the electrode. In other tested electrolytes, such behavior has not been observed.

Electrolytes of the third generation, $Mg[X(hfip)_4]_2$, perform with the lowest overpotentials below 0.1 V after 10 cycles, followed by the APC electrolyte with 0.15 V. TFSI-based electrolytes exhibit significantly higher values, around 0.3 V. Since all electrolytes exhibit rather similar ionic conductivities (3-6 mS cm^{-1}),[9,20,31] the difference in overpotentials likely stems from variations in the metal–electrolyte interphase rather than bulk electrolyte resistance. Due to the large overpotentials in the first plating half-cycle in TFSI-based electrolytes, the potential window was extended to a lower potential limit of –2.5 V to initiate the first plating on the working electrode. Large initial overpotentials are attributed to the partial electrode passivation caused by the $TFSI^-$ anion decomposition, which is not fully mitigated by the presence of chloride species. Moreover, $Mg(TFSI)_2$ salt is hydrophilic, and despite extensive drying of the salt before use, trace water cannot be fully removed. Water reduction on the Mg metal surface can contribute to increased overpotentials due to the formation of MgO, $Mg(OH)_2$, and other species.[32] On the other hand, organometallic species in the APC electrolyte can scavenge protic impurities, resulting in the electrolyte performing with half smaller overpotentials. An additional decrease of overpotentials in $Mg[X(hfip)_4]_2$ electrolytes is attributed to the more facile salt dissociation and high reductive stability of $[X(hfip)_4]^-$ anions. At the same time, it should be noted that the $Mg[X(hfip)_4]_2$ salts were synthesized using a highly controlled synthesis approach, resulting in a high purity of the Mg salts and a very low water content.[33,34] Although the standard cycling protocol provides insights into cell reversibility to some extent, a relatively small number of cycles and modest current density (1 mA cm^{-2}) may fail to fully reveal all the side reactions.

To increase the exposure of Mg metal deposits on the working electrode to electrolytes throughout the cycling procedure, as well as minimize potential variations on the working electrode, particularly at the end of the Mg stripping process, macroreversibility cycling was employed. In APC and $Mg[X(hfip)_4]_2$ electrolytes, the measurements followed the intended protocol; that is, the initially plated Mg served as a reservoir and was completely stripped from the working electrode only in the final stripping cycle (Figure S2, Supporting Information). In intermediate cycles, the cycling resembles an Mg||Mg symmetrical cell, with the upper potential limit during intermittent Mg stripping from the working electrode not being reached. In contrast, cells using $Mg(TFSI)_2$:$MgCl_2$ electrolytes reached the potential limit at 1.5 V after only 15 and 9 cycles in 1:1 and 1:0.5 electrolyte compositions, respectively (Figure S3, Supporting Information). This indicates that no active Mg metal deposits remained on the working electrode during intermediate cycles, and the initially plated Mg became either fully passivated or had completely reacted with the electrolyte. The lower cycle number was observed in the electrolyte with less $MgCl_2$, suggesting the side reactions are impeded by the presence of $MgCl_2$. This is in good agreement with standard cycling and literature results, where the electrolyte with the higher ratio of $MgCl_2$ exhibited favorable performance due to the enhanced prevention of the $TFSI^-$ anion decomposition compared to electrolytes containing a lower amount of $MgCl_2$.[29]

The comparison of average Coulombic efficiencies under standard and macroreversibility cycling protocols in different electrolytes is presented in **Table 1**. All measurements were conducted using three parallel cells, with the listed values representing the average of three measurements along with their corresponding standard deviations. Under the macroreversibility

Table 1. Average Coulombic efficiencies after 100 cycles of Mg plating/stripping in selected electrolytes using standard and macroreversibility cycling protocols and corresponding standard deviations for three parallel cells.

Electrolyte	Average Coulombic efficiency (%)			
	Standard	σ	Macroreversibility	σ
APC	99.1	0.2	99.5	0.1
$Mg(TFSI)_2$:$MgCl_2$ = 1:1	90.6	0.3	87.9	0.7
$Mg(TFSI)_2$:$MgCl_2$ = 1:0.5	79.8	0.3	78.1	0.3
$Mg[Al(hfip)_4]_2$	98.1	0.4	98.5	0.2
$Mg[B(hfip)_4]_2$	96.3	0.4	98.2	0.2

protocol, the average Coulombic efficiency over 100 cycles in TFSI-based electrolytes is ≈1%–3% lower compared to the standard cycling protocol, confirming the instability of the metal/electrolyte interphase in these systems. Conversely, the $Mg[B(hfip)_4]_2$ electrolyte exhibits a higher average Coulombic efficiency (1%–2%) under the macroreversibility protocol relative to standard cycling. This could be attributed to the enhanced adhesion of Mg deposits to the predeposited Mg layer compared to the stainless steel working electrode, as well as a more stable potential at the working electrode, both of which could contribute to a more stable Mg metal/electrolyte interphase. For APC and $Mg[Al(hfip)_4]_2$ electrolytes, the average Coulombic efficiency shows a marginal increase under macroreversibility cycling conditions, although the differences remain close to the range of the standard deviation.

While the macroreversibility cycling protocol confirms the limited stability of $Mg(TFSI)_2$-based electrolytes and their progressive degradation over cycling, the performance of other electrolytes under these conditions is quite comparable to the standard protocol. This motivated additional experiments under closer to real-life operating conditions by extending the contact time between the electrolyte and Mg deposits during OCV rest periods.

The measurements with different OCV periods after each Mg plating are shown in **Figure 4**. The introduction of OCV periods leads to a decrease in Coulombic efficiency for all tested electrolytes. The decrease becomes more significant upon longer OCV durations, indicating progressive Mg metal passivation/corrosion over time. In APC and $Mg[Al(hfip)_4]_2$ electrolytes, the decrease is moderate, and cycling with 5 h OCV shows 1%–2% lower Coulombic efficiency compared to the standard cycling (Table S1, Supporting Information). The $Mg[B(hfip)_4]_2$ electrolyte exhibits a more pronounced decline in reversibility with extended OCV periods, suggesting a higher degree of Mg passivation/corrosion compared to the aluminate analog. The performance of $Mg(TFSI)_2$-based electrolytes varies significantly depending on the stoichiometry of $MgCl_2$. Interestingly, the electrolyte with a 1:1 ratio of salts shows only a minor decrease in Coulombic efficiency, even after extended OCV periods. In contrast, the 1:0.5 electrolyte exhibits rapid performance degradation, and after introducing 2 h OCV periods, the stripping overpotential sharply increases, reaching the cutoff potential limit at less than 0.05 mAh cm^{-2} of capacity (Figure S4, Supporting Information). This suggests near-complete electrode passivation/corrosion after prolonged exposure of Mg deposits to the electrolyte. Other Mg electrolytes display much smaller changes in overpotentials with cycling (Figure S5, Supporting Information). In APC and $Mg[X(hfip)_4]_2$ electrolytes, the changes are minimal, while an increase is observed in $Mg(TFSI)_2$:$MgCl_2$ = 1:1 electrolyte with rest periods, compared to standard cycling.

While macroreversibility measurements of the $Mg(TFSI)_2$:$MgCl_2$ = 1:1 electrolyte suggest that Mg deposits undergo gradual passivation during cycling, test with OCV periods indicates that the formed interfacial layer remains relatively stable when Mg deposits are exposed to the electrolyte for an extended time during OCV rest. More importantly, cycling with OCV periods reveals some degree of passivation/corrosion in all Mg electrolytes, phenomena not detected by standard and macroreversibility measurements, where cells are under constant current load. Mg plating/stripping with included rest periods can serve as an additional diagnostic tool for the characterization of electrolytes under more practically relevant conditions, which has been rarely used in the past.[14,25] The obtained results highlight a clear need for further development of Mg electrolytes to stabilize the Mg metal/electrolyte interphase during rest periods.

Mg deposits in different electrolytes were characterized by SEM-EDX and XPS. In all the electrolytes examined, SEM imaging at high magnification shows hexagonal-shaped deposits with sharp edges and high crystallinity. In the APC electrolyte, deposits retain the angular structure up to 1 μm in size, while in electrolytes of second and third generations, deposits agglomerate into larger structures (10 μm and larger) of different shapes and morphologies (Figure S6, Supporting Information). The EDX analysis of APC deposits shows a high content of Mg metal (94.4%, Table S2, Supporting Information), which aligns with a high Coulombic efficiency for Mg plating/stripping in this electrolyte. The low C and O content is probably due to contamination of the microscope rather than decomposition of the APC electrolyte, which should display also the presence of Cl and Al species. The Mg metal content of the deposits in both TFSI-based electrolytes is lower compared to APC, ranging between 85% and 90%. Additionally, N and S were detected, indicating $TFSI^-$ anion decomposition. The electrolyte with $Mg(TFSI)_2$:$MgCl_2$ ratio of 1:0.5 shows a somewhat higher S content, corresponding to a higher degree of $TFSI^-$ anion decomposition compared to the analog with more $MgCl_2$, further confirming the positive effect of $MgCl_2$. In $Mg[Al(hfip)_4]_2$ and $Mg[B(hfip)_4]_2$ electrolytes, the deposits consist of 91% and 84% of Mg, respectively. Besides C and O, F is also detected, which indicates a certain degree of $[X(hfip)_4]^-$ anion decomposition or its presence in the Mg metal/electrolyte interphase. Notably, deposits in $Mg[Al(hfip)_4]_2$ contain more Mg and lower amounts of additional elements (O, C, and F) compared to the $Mg[B(hfip)_4]_2$. This suggests a more electrolyte decomposition of the latter, which aligns with its inferior electrochemical performance and lower Coulombic efficiency over the alkoxyaluminate-based analog observed in this work, as well as in the recent literature reports.[20]

The XPS Mg 2p spectra of Mg deposits (**Figure 5** and S7, Supporting Information) were analyzed to gain insight into the interphase of Mg metal deposits, with brushed Mg foil

Research Article
doi.org/10.1002/batt.202500265
Chemistry Europe
European Chemical Societies Publishing

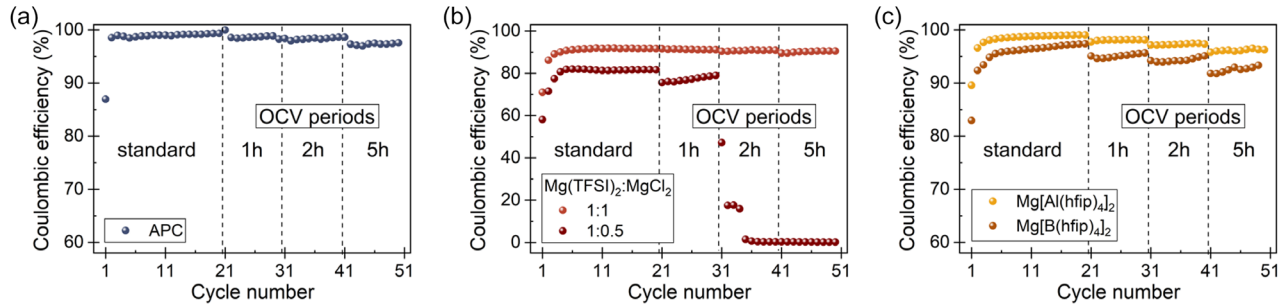

Figure 4. Comparison of cycling with OCV periods. Coulombic efficiency of Mg plating/stripping in selected electrolytes: a) APC in THF, b) $Mg(TFSI)_2$:$MgCl_2$ in 1:1 and 1:0.5 ratios in G2, and **c)** $Mg[Al(hfip)_4]_2$ and $Mg[B(hfip)_4]_2$ in G2.

additionally included as a reference sample. Details of the XPS spectra fitting procedure are described in the SI and summarized in Table S3, Supporting Information. The Mg 2p spectrum of brushed Mg foil displays a clear metallic Mg contribution, along with a very intense MgO contribution. This composition of Mg foil was found reproducible and could be attributed to the incomplete removal of MgO layer through the brushing procedure, as well as the rapid passivation of Mg metal upon contact with traces of O_2 and solvents inside the glove box, leading to the formation of a thin MgO layer. The composition of Mg metal/electrolyte interphase is attributed to the decomposition/adsorption of electrolyte species on the surface of Mg metal, correlating strongly to the electrolyte composition and cation solvation shell. In the APC electrolyte, deposits have the most pronounced metallic character, consistent with its best electrochemical performance. The metallic character decreases when moving to $Mg[X(hfip)_4]_2$ electrolytes, with the boron analog displaying a higher contribution of metallic Mg. This contrasts with EDX results, which show relatively higher Mg content in $Mg[Al(hfip)_4]_2$. However, it is important to note that while EDX provides more bulk composition information, XPS specifically probes the surface species in the depths of down to 5–10 nm. Both $Mg[X(hfip)_4]_2$ electrolytes also show contributions from MgO and MgF_2, which are more present in $Mg[Al(hfip)_4]_2$. Less-metallic Mg deposits, yet the best electrochemical performance of the $Mg[Al(hfip)_4]_2$ electrolyte compared to its boron analog suggests a favorable interphase composition that may play a crucial role in facilitating efficient Mg plating/stripping in Mg alkoxyaluminates. The metallic Mg signal is the lowest in both $Mg(TFSI)_2$:$MgCl_2$-based electrolytes, which contain significant contributions of MgO and MgF_2, confirming intense decomposition at the Mg metal interphase. Surprisingly, the better-performing $Mg(TFSI)_2$:$MgCl_2$ = 1:1 electrolyte displays lower metallic contribution and a clear $MgCl_2$ signal that could not be fitted into the Mg 2p spectrum of metal deposits from the $Mg(TFSI)_2$:$MgCl_2$ = 1:0.5 electrolyte. This points to the fact that $MgCl_2$ becomes prominent in the Mg interphase in the $Mg(TFSI)_2$:$MgCl_2$ = 1:1 and is most likely the key reason for a significant

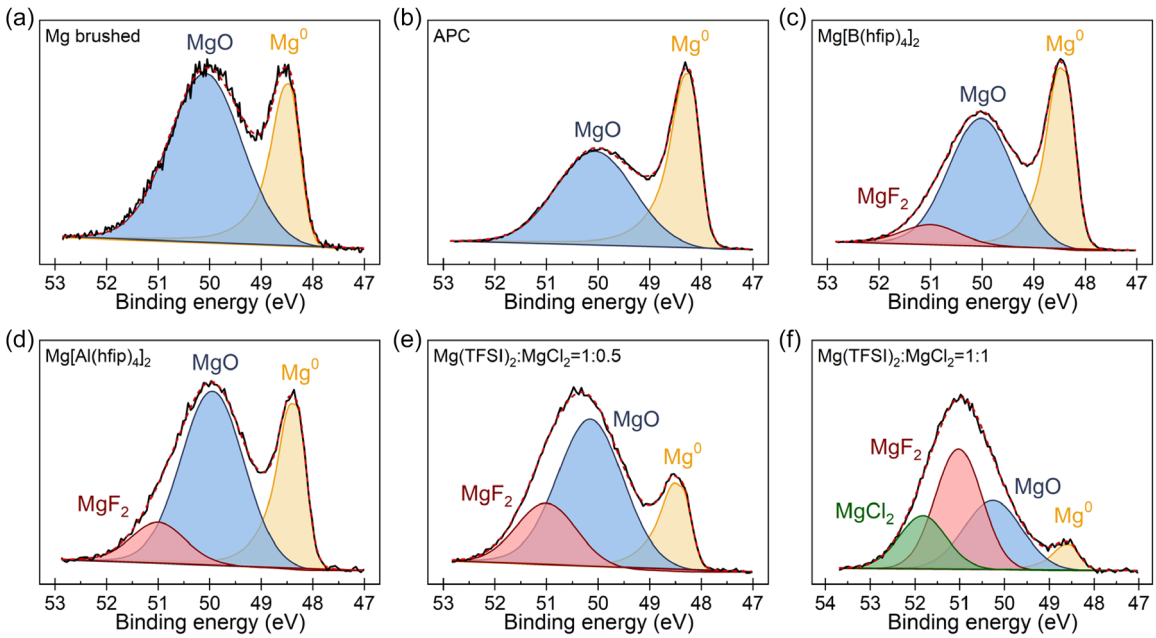

Figure 5. XPS Mg 2p spectra of brushed Mg foil and Mg deposits in 0.4 M Mg electrolytes: a) Mg foil brushed inside the glove box, b) APC, c) $Mg[B(hfip)_4]_2$, d) $Mg[Al(hfip)_4]_2$, e) $Mg(TFSI)_2$:$MgCl_2$ = 1:0.5, and f) $Mg(TFSI)_2$:$MgCl_2$ = 1:1. The solid black and dashed red lines represent the measured and fitted XPS spectra, respectively. XPS spectra are fitted with contributions assigned to metallic Mg (yellow), MgO (blue), MgF_2 (red), and $MgCl_2$ (green) species.

improvement of the electrochemical behavior in this electrolyte.[14,35] At the same time, a lower Mg metal contribution in $Mg(TFSI)_2$:$MgCl_2 = 1{:}1$, similar as in the case of $Mg[Al(hfip)_4]_2$, points to the fact that a more metallic character of Mg metal interphase does not necessarily result in better Mg plating/stripping performance. This is also supported by results of Mg plating/stripping with OCV rest periods, where $Mg(TFSI)_2$:$MgCl_2 = 1{:}1$ and $Mg[Al(hfip)_4]_2$ display a lower drop in Mg plating/stripping efficiency than $Mg(TFSI)_2$:$MgCl_2 = 1{:}0.5$ and $Mg[B(hfip)_4]_2$ electrolytes. While MgO is generally considered a detrimental surface species as it exhibits a very high barrier for Mg^{2+} migration, MgF_2 can enable Mg^{2+} transfer with a much lower migration barrier, while limiting electrolyte decomposition.[36,37] Similarly, adsorption of $MgCl_2$ species on Mg metal has also shown a positive effect on the reversibility of Mg metal plating/stripping and improved tolerance to electrolyte impurities.[14,35]

3. Conclusions

The development of Mg electrolytes has made considerable progress over the last two decades, bringing Mg batteries closer to practical application. In this work, a comprehensive benchmarking of three generations of Mg electrolytes is performed through three different electrochemical metal plating/stripping protocols, supported by SEM, EDX, and XPS characterization of Mg metal deposits. Standard galvanostatic Mg plating/stripping tests are complemented by macroreversibility cycling and cycling with OCV periods. Results show that the current best-performing weakly coordinating anion (WCA)-based salt, $Mg[Al(hfip)_4]_2$, delivers plating/stripping Coulombic efficiency close to the organometallic APC electrolyte, with a lower plating/stripping overpotential. Its analog, $Mg[B(hfip)_4]_2$, displays slightly lower Coulombic efficiency while maintaining a similar overpotential. The second-generation $Mg(TFSI)_2$:$MgCl_2$ electrolytes demonstrate inferior performance, especially at a $Mg(TFSI)_2$:$MgCl_2$ ratio of 1:0.5. An important finding is that Mg plating/stripping tests with OCV periods show a decrease in Mg plating/stripping efficiency in all tested electrolytes, which is particularly detrimental for the worst-performing $Mg(TFSI)_2$:$MgCl_2$ electrolyte. Tests with OCV rest periods indicate Mg metal passivation/corrosion in all used electrolytes, which should be addressed in future development of Mg electrolytes. XPS analysis reveals the most pronounced metallic character of Mg deposits in APC, whereas the interphase in the second- and third-generation electrolytes exhibits a prevalent character corresponding to Mg^{2+} species. Higher plating/stripping efficiency in $Mg[Al(hfip)_4]_2$ and $Mg(TFSI)_2$:$MgCl_2$=1:1 electrolytes despite less-metallic characters as their counterparts, $Mg[B(hfip)_4]_2$ and $Mg(TFSI)_2$:$MgCl_2$=1:0.5, respectively, points to a beneficial effect of MgF_2 and $MgCl_2$ species in the Mg metal/electrolyte interphase, which should be explored in the future as both electrolytes exhibit also relatively smaller drops in efficiency during OCV rest periods. We believe that further improvements of Mg plating/stripping toward the required 99.9%+ Coulombic efficiency can be achieved by specifically targeting the composition of the Mg metal interphase, as many combinations of Mg salts and additives remain unexplored.

Benchmarking Mg electrolytes through different electrochemical protocols within this work underscores the need to complement the current standard constant current load with additional protocols, such as those including rest periods, which are more sensitive toward different metal anode passivation/corrosion processes. Moreover, the role of different working electrode substrates warrants investigation, as substrate choice can significantly influence the adhesion and growth of Mg metal deposits.[38] While Pt metal remains the literature standard due to its corrosion resistance, which is needed to study Mg electrolytes of first and second generations, future work should move toward more common metals that could be used in practical battery cells.

4. Experimental Section

Electrolytes

Syntheses, preparation of electrolytes, and cell assembling were performed under an inert atmosphere in an argon-filled glove box with oxygen and water levels below 1 ppm.

All electrolytes were prepared at a total Mg^{2+} ion concentration of 0.4 M. Tetrahydrofuran (THF, 99.9%, Wako Chemicals) and diglyme (G2, 99%, Acros Organics) solvents underwent a purification/drying procedure before use, including drying with 4 Å molecular sieves (3–4 days), reflux with Na/K alloy (1/3 wt%), and fractional distillation. The water content in the as-dried solvents was determined by Karl Fischer titration to be below 1 ppm.

The APC electrolyte was prepared using a standard literature procedure, which involved mixing the PhMgCl and $AlCl_3$ in a 2:1 ratio.[39] PhMgCl (2 M in THF, Sigma Aldrich) was slowly added to $AlCl_3$ (anhydrous, 99.985%, Alfa Aesar) dissolved in THF. The solution was diluted with THF and stirred overnight.

TFSI-based electrolytes were prepared by weighing the appropriate amount of commercial $Mg(TFSI)_2$ (99.5%, Solvionic) and $MgCl_2$ (ultradry, 99.99%, Alfa Aesar) salts in 1:1 or 1:0.5 ratios into a measuring flask and diluting it up to the mark with a G2 solvent. Electrolytes were stirred at room temperature overnight. Note that $Mg(TFSI)_2$ was vacuum dried at 250 °C for a few days before use to reduce the water content in the commercial salt.

$Mg[B(hfip)_4]_2$ and $Mg[Al(hfip)_4]_2$ salts were synthesized through previously published procedures.[17] Salts were weighed into a measuring flask and dissolved in G2 solvent. Electrolytes were stirred at room temperature overnight.

Cell Assembly

Two-electrode Swagelok-type cells were assembled with the Mg counter and stainless steel (SS) WE. Mg foil (0.1 mm, 99.95%, Changsha Rich Nonferrous Metals) was polished with P1200 sandpaper before use. Between the electrodes, three glass fiber separators (GF/A 260 μm, Whatman) were placed and wetted with ≈80 μL of the Mg electrolyte. Note that cells with $Mg(TFSI)_2$:$MgCl_2$ electrolyte 1:0.5 ratio short circuited after a few cycles when being assembled with three separators between the working and counter electrode. Thus, an additional separator was used in these cells with a specific electrolyte composition. The amount of the electrolyte was adjusted accordingly (100 μL).

Electrochemical Characterization

Electrochemical testing was performed under galvanostatic mode with a VMP3 potentiostat from Bio-Logic. The performance of selected electrolytes was investigated through three different cycling protocols. The first, standard galvanostatic protocol for Mg batteries included Mg plating at 1 mA cm^{-2} for 12 min (0.2 mAh cm^{-2}) and stripping with the same current density until a cutoff voltage of 1.5 V. The upper potential was limited due to the corrosion of chloride-containing electrolytes at high potentials. The second protocol, so-called macroreversibility cycling, consisted of Mg plating at 1 mA cm^{-2} for 1 h (1 mAh cm^{-2}), during which a larger amount of Mg was plated, followed by continuous plating/stripping of only 20% of the initially plated Mg metal (1 mA cm^{-2}, 0.2 mAh cm^{-2}). After 95 cycles, the remaining Mg metal was stripped until a cutoff voltage of 1.5 V. Note that macroreversibility cycling only allowed the calculation of average Coulombic efficiency throughout the whole cycling, rather than the calculation of the efficiency of the individual cycles. The third cycling protocol was similar to the first one but included OCV rest periods (1, 2, and 5 h) after Mg plating. To ensure the reproducibility of results, all of the galvanostatic Mg plating/stripping measurements were performed in three parallel cells.

Characterization of Deposits

Samples of Mg deposits for SEM–EDX analysis were prepared by Mg plating on the stainless steel substrate at 1 mA cm^{-2} current density for 12 min (0.2 mAh cm^{-2}). When assembling the cells, an additional Celgard 2400 separator was placed on the working electrode side to prevent the entanglement of glass fibers with Mg metal deposits. After electrochemical deposition, cells were transferred back to the glove box and disassembled. The substrate was rinsed with G2 solvent to remove electrolyte residues. Samples were taken to the SEM chamber using a vacuum sample holder to prevent exposure to air and moisture. SEM–EDX analyses were performed on an SEM Supra 35 VP from Carl Zeiss at 20 kV with the Ultim Max 100 (Oxford) EDX detector.

X-Ray Photoelectron Spectroscopy

Ex situ XPS analysis was performed on a brushed Mg foil reference and Mg deposits formed in different electrolytes upon Mg plating at a current density of 1 mA cm^{-2} for 1 h on a carbon-coated Al foil substrate. After Mg plating, cells were disassembled, and the substrate was rinsed with G2 solvent to remove electrolyte residues. Brushed Mg metal and substrate with deposits were placed on a nonconductive double-sided scotch tape in a floating setup and positioned at the center of the XPS holder. All sample handling was carried out in an argon-filled glove box. After mounting, samples were transferred into the XPS intro chamber using a transfer vessel to avoid air exposure. Measurements were conducted using a VersaProbe III-AD (Physical Electronics) with a monochromatic Al Kα X-ray source operating at 15 kV and 13.3 mA. For each sample, high-resolution spectra were acquired by scanning a 1×1 mm^2 area with a beam size of 200 μm at a pass energy of 27 eV and a step of 0.05 eV to obtain high-quality data. Peak analysis was performed with the MultiPak software using a weighted sum of Lorentzian and Gaussian component curves after Shirley background subtraction. Binding energies were referenced to the internal C1s standard at 284.6 eV.

Acknowledgements

The authors would like to acknowledge the financial support of the Slovenian Research and Innovation Agency (ARIS) through research program P2-0423, as well as projects N2-0279 and J2-4462.

Conflict of Interest

The authors declare no conflict of interest.

Data Availability Statement

The data that support the findings of this study are available from the corresponding author upon reasonable request.

Keywords: different cycling procedures · metal/electrolyte interphases · Mg electrolytes · Mg plating/stripping

[1] J.-M. Tarascon, M. Armand, *Nature* **2001**, *414*, 359.
[2] Y. Liang, H. Dong, D. Aurbach, Y. Yao, *Nat. Energy* **2020**, *5*, 646.
[3] M. Jäckle, A. Groß, *J. Chem. Phys.* **2014**, *141*, 174710.
[4] A. Ponrouch, J. Bitenc, R. Dominko, N. Lindahl, P. Johansson, M. R. Palacin, *Energy Storage Mater.* **2019**, *20*, 253.
[5] Z. Lu, A. Schechter, M. Moshkovich, D. Aurbach, *J. Electroanal. Chem.* **1999**, *466*, 203.
[6] L. W. Gaddum, H. E. French, *J. Am. Chem. Soc.* **1927**, *49*, 1295.
[7] D. Aurbach, Z. Lu, A. Schechter, Y. Gofer, H. Gizbar, R. Turgeman, Y. Cohen, M. Moshkovich, E. Levi, *Nature* **2000**, *407*, 724.
[8] R. Attias, M. Salama, B. Hirsch, Y. Goffer, D. Aurbach, *Joule* **2019**, *3*, 27.
[9] O. Mizrahi, N. Amir, E. Pollak, O. Chusid, V. Marks, H. Gottlieb, L. Larush, E. Zinigrad, D. Aurbach, *J. Electrochem. Soc.* **2008**, *155*, A103.
[10] C. Liebenow, Z. Yang, P. Lobitz, *Electrochem Commun.* **2000**, *2*, 641.
[11] S. Y. Ha, Y. W. Lee, S. W. Woo, B. Koo, J. S. Kim, J. Cho, K. T. Lee, N. S. Choi, *ACS Appl. Mater. Interfaces* **2014**, *6*, 4063.
[12] H. S. Kim, T. S. Arthur, G. D. Allred, J. Zajicek, J. G. Newman, A. E. Rodnyansky, A. G. Oliver, W. C. Boggess, J. Muldoon, *Nat. Commun.* **2011**, *2*, 427.
[13] Y. Cheng, R. M. Stolley, K. S. Han, Y. Shao, B. W. Arey, N. M. Washton, K. T. Mueller, M. L. Helm, V. L. Sprenkle, J. Liu, G. Li, *Phys. Chem. Chem. Phys.* **2015**, *17*, 13307.
[14] J. G. Connell, B. Genorio, P. P. Lopes, D. Strmcnik, V. R. Stamenkovic, N. M. Markovic, *Chem. Mater.* **2016**, *28*, 8268.
[15] J. Muldoon, C. B. Bucur, A. G. Oliver, J. Zajicek, G. D. Allred, W. C. Boggess, *Energy Environ Sci* **2013**, *6*, 482.
[16] W. Ren, M. Cheng, Y. Wang, D. Zhang, Y. Yang, J. Yang, J. Wang, Y. NuLi, *Batter Supercaps* **2022**, *5*, e202200263.
[17] T. Pavčnik, M. Lozinšek, K. Pirnat, A. Vizintin, T. Mandai, D. Aurbach, R. Dominko, J. Bitenc, *ACS Appl Mater Interfaces* **2022**, *14*, 26766.
[18] O. Tutusaus, R. Mohtadi, T. S. Arthur, F. Mizuno, E. G. Nelson, Y. V. Sevryugina, *Angewandte Chemie Int. Ed.* **2015**, *54*, 7900.
[19] Y. Shao, N. N. Rajput, J. Hu, M. Hu, T. Liu, Z. Wei, M. Gu, X. Deng, S. Xu, K. S. Han, J. Wang, Z. Nie, G. Li, K. R. Zavadil, J. Xiao, C. Wang, W. A. Henderson, J. G. Zhang, Y. Wang, K. T. Mueller, K. Persson, J. Liu, *Nano Energy* **2015**, *12*, 750.
[20] T. Mandai, Y. Youn, Y. Tateyama, *Mater. Adv.* **2021**, *2*, 6283.
[21] Z. Zhao-Karger, M. E. Gil Bardaji, O. Fuhr, M. Fichtner, *J. Mater. Chem. A Mater.* **2017**, *5*, 10815.
[22] D. Aurbach, O. Youngman, Y. Gofer, A. Meitav, *Electrochim Acta* **1990**, *35*, 625.
[23] M. Salama, R. Attias, B. Hirsch, R. Yemini, Y. Gofer, M. Noked, D. Aurbach, *ACS Appl. Mater. Interfaces* **2018**, *10*, 36910.
[24] R. Attias, B. Dlugatch, O. Blumen, K. Shwartsman, M. Salama, N. Shpigel, D. Sharon, *ACS Appl. Mater. Interfaces* **2022**, *14*, 30952.
[25] I. Shterenberg, M. Salama, H. D. Yoo, Y. Gofer, J.-B. Park, Y.-K. Sun, D. Aurbach, *J. Electrochem Soc.* **2015**, *162*, A7118.
[26] L. Ma, M. A. Schroeder, T. P. Pollard, O. Borodin, M. S. Ding, R. Sun, L. Cao, J. Ho, D. R. Baker, C. Wang, K. Xu, *Energy and Environm. Mater.* **2020**, *3*, 516.
[27] L. Ma, M. A. Schroeder, O. Borodin, T. P. Pollard, M. S. Ding, C. Wang, K. Xu, *Nat. Energy* **2020**, *5*, 743.
[28] Z. Yang, M. Yang, N. T. Hahn, J. Connell, I. Bloom, C. Liao, B. J. Ingram, L. Trahey, *Front. Chem.* **2022**, *10*, 937.
[29] N. Sa, B. Pan, A. Saha-Shah, A. A. Hubaud, J. T. Vaughey, L. A. Baker, C. Liao, A. K. Burrell, *ACS Appl. Mater. Interfaces* **2016**, *8*, 16002.
[30] B. Dlugatch, M. Mohankumar, R. Attias, B. M. Krishna, Y. Elias, Y. Gofer, D. Zitoun, D. Aurbach, *ACS Appl. Mater. Interfaces* **2021**, *13*, 54894.

[31] N. Sa, N. N. Rajput, H. Wang, B. Key, M. Ferrandon, V. Srinivasan, K. A. Persson, A. K. Burrell, J. T. Vaughey, *RSC Adv.* **2016**, *6*, 113663.
[32] J. G. Connell, B. Genorio, P. P. Lopes, D. Strmcnik, V. R. Stamenkovic, N. M. Markovic, *Chem. Mater.* **2016**, *28*, 7.
[33] T. Pavčnik, J. Imperl, M. Kolar, R. Dominko, J. Bitenc, *J. Mater. Chem. A Mater.* **2024**, *12*, 3386.
[34] T. Mandai, *ACS Appl. Mater. Interfaces* **2020**, *12*, 39135.
[35] B. W. Schick, V. Vanoppen, M. Uhl, M. Kruck, S. Riedel, Z. Zhao-Karger, E. J. Berg, X. Hou, T. Jacob, *Angewandte Chemie Int. Ed.* **2024**, *63*, e202413058.
[36] J. Forero-Saboya, C. Davoisne, R. Dedryvère, I. Yousef, P. Canepa, A. Ponrouch, *Energy Environ. Sci.* **2020**, *13*, 3423.
[37] B. Li, R. Masse, C. Liu, Y. Hu, W. Li, G. Zhang, G. Cao, *Energy Storage Mater.* **2019**, *22*, 96.
[38] M. Radi, T. Purkait, D. S. Tchitchekova, A. R. Goñi, R. Markowski, C. Bodin, C. Courrèges, R. Dedryvère, A. Ponrouch, *Adv. Energy Mater.* **2024**, *14*, 2401587.
[39] N. Pour, Y. Gofer, D. T. Major, D. Aurbach, *J. Am. Chem. Soc.* **2011**, *133*, 6270.

Manuscript received: April 8, 2025
Revised manuscript received: June 20, 2025
Version of record online: